Articles

Examination of Size-Induced Ferroelectric Phase Transitions in Template Synthesized $PbTiO_3$ Nanotubes and Nanofibers

Bernadette A. Hernandez-Sanchez, Ki-Seog Chang, Michael T. Scancella, Jennifer L. Burris, Sandeep Kohli, Ellen R. Fisher, and Peter K. Dorhout*

Department of Chemistry, Colorado State University, Fort Collins, Colorado 80523

Received April 14, 2004. Revised Manuscript Received June 9, 2005

Here we report on the application of sol−gel template synthesis to the investigation of size-induced ferroelectric phase transitions in lead titanate ($PbTiO_3$) nanotubes and nanofibers. A 0.8 M chelate sol−gel, made from titanium(IV) tertabutoxide and lead(II) trihydrate acetate, was applied to two different templates. Nanotubes were formed within 200-nm-pore Whatman anodisc aluminum oxide membranes, and nanofibers were prepared using 50-, 100-, and 200-nm Whatman track-etched polycarbonate membranes. Transmission electron microscopy images revealed that the tubes comprised grains of $\leq$20 nm and the fibers comprised individual grains $\leq$200 nm in width when a 200-nm pore size template is used. An examination of how the grain/crystallite size and aspect ratio of one-dimensional morphologies affect the ferroelectric phase transition was monitored through the comparison of bulk powders and the nanostructured materials using electron diffraction, X-ray diffraction, Raman spectroscopy, and differential scanning calorimetry.

I. Introduction

One-dimensional (1-D) metal oxides are of significant interest in the research and development of nanotechnology.[1−3] The morphologies of 1-D materials, which include tubes, rods, fibers, and wires, provide unique systems in which the investigation of both aspect ratio and dimensionality can be examined.[4] One approach to an investigation is to systematically produce and study the physical properties of 1-D morphologies derived from the assistance of well-defined templates that ensure control over parameters such as the diameter and length of the materials in question. In an initial communication, we reported the preliminary results for an experimental investigation on how sol−gel synthesis could be applied to a template to affect the preparation of nanometer-sized perovskite materials.[5] Our experiments demonstrated that template synthesis not only aided in the control over the geometrical constraints but also constricted the grain/crystallite size of the perovskites. Our procedure generated interesting models for the examination of size effects that occur with perovskite ceramics having grain sizes below 1.0 μm.

The influence of crystal chemistry and size on the properties of ferroelectric perovskites is of general concern because of the interest in fabricating micro- and nanoscale electronic components. Prior research on ferroelectric ceramics had found the following deviations in polycrystalline samples with grain sizes below 1.0 μm: a decrease in the lattice parameter ratio (c/a) for the ferroelectric unit cell and a decrease in both the ferroelectric phase transition temperature (T_c) and the enthalpy (H), which caused a decrease in polarization and dielectric constants.[6,7] These size effects have been observed in both bulk powder and thin film morphologies, and the fundamental source of the size effects is still unclear. Several possible mechanisms have been proposed to explain the effects of particle size on the ferroelectric phase transition temperature in perovskites. These have included depolarization effects, the absence of long-range cooperative interactions, structural defects, and elastic constraints.[7]

Among the many commercially relevant displacive ferroelectrics, the $PbTiO_3$−$PbZrO_3$ (PZT) solid solution system is well-suited for our studies. Thus, we have begun our investigation on this system by producing nanotubes and fibers of $PbTiO_3$. In contrast to $BaTiO_3$, few studies have appeared that address size effects in $PbTiO_3$ systems.[8−21]

(1) Patzke, G.; Krumeich, F.; Nesper, R. *Angew. Chem., Int. Ed.* **2003**, *41*, 2446−2461.
(2) Rao, C. N. R.; Nath, M. *Dalton Trans.* **2003**, *1*, 1−24.
(3) Rao, C. N. R.; Deepak, F. L.; Gundiah, G.; Govindaraj, A. *Prog. Solid State Chem.* **2003**, *31*, 5−147.
(4) Xia, Y.; Yang, P.; Sun, Y.; Wu, Y.; Mayers, B.; Gates, B.; Yin, Y.; Kim, F.; Yan, H. *Adv. Mater.* **2003**, *15*, 353−388.
(5) Hernandez, B. A.; Chang, K.-S.; Fisher, E. R.; Dorhout, P. K. *Chem. Mater.* **2002**, *14*, 480−482.
(6) Akdogan, E. K.; Leonard, M. R.; Safari, A. In *Handbook of Low and High Dielectric Constant Materials and Their Applications*; Nawala, H. S., Ed.; Academic Press: New York, 1999; Vol. 2, pp 61−112.
(7) Frey, M. H.; Payne, D. A. *Phys. Rev. B* **1996**, *54*, 3158−3168.
(8) Akdogan, E. K.; Mayo, W.; Safri, A.; Rawn, C. J.; Payzant, E. A. *Ferroelectrics* **1999**, *223*, 11−18.

10.1021/cm0493896 CCC: $30.25
Published on Web 11/03/2005

Here we report on the examination of the ferroelectric phase transition of $PbTiO_3$ nanotubes and nanofibers as the particle size and potentially the aspect ratio are controlled. To our knowledge, this is the first report on size-induced ferroelectric phase transition temperature (T_c) deviations for 1-D constrained perovskites.

Recently, four independent research groups led by Cao,[22−25] Park,[26,27] Mallouk,[28] and Wong[29] have reported on the synthesis and characterization of 1-D perovskite materials. In addition to their nanoparticle counterparts, 1-D perovskites have become excellent models to investigate how the ferroelectric crystal structure and state of polarization may be influenced by size and dimensionality by allowing for a unique geometrical constraint on domain behavior. The Park group demonstrated that single-crystalline $BaTiO_3$ nanowires with diameters of 10−60 nm could be polarized under vacuum conditions using scanning probe techniques.[27] The wires had ferroelectric domains, dimensions of several nanometers along the *c* axis, which were used to write and store information. These results are relevant to the investigation of size effects by experimentally contributing to the identification of a critical size that is lower than what was previously reported. Using nanoparticle models, Wang et al. determined the critical size of $BaTiO_3$ by Landau−Devonshire theory to be 44 nm, whereas Akdogan and Safri experimentally determined this value to be 67 nm through extrapolation.[19,30]

The ferroelectric $PbTiO_3$ system was also well-suited for our studies because of its relatively low processing temperature for the chelate sol−gel method (between 450 and 800 °C) versus $BaTiO_3$ (above 1100 °C).[7,31,32] The processing temperature needed to obtain the ferroelectric phase is critical in considering the stability of the alumina template used to form the submicrometer-sized particles. Synthetic processing conditions and the effects of crystallite size on the ferroelectric transition temperature of one-dimenisonal perovskites will be addressed in this article.

II. Experimental Methods

Materials. Titanium(IV) tetrabutoxide ($Ti[O(CH_2)_3CH_3]_4$) and lead(II) trihydrate acetate, $Pb(CH_3CO_2)_2 \cdot 3H_2O$, were purchased from Aldrich and were used as received. Glacial acetic acid (CH_3CO_2H), 1-butanol ($CH_3(CH_2)_3OH$), Whatman anodisc aluminum oxide (AAO) membranes (200-nm pore size, 50-μm thick, 25-mm diameter, 100 ± 30 nm pore-to-pore distance), Whatman track-etched polycarbonate (PC) membranes with pore sizes of 200, 100, and 50 nm (10-μm thick, 25-mm diameter, 690 ± 360 nm pore-to-pore distance), and CoorsTek combustion boats were purchased from Fisher. To prevent or minimize the formation of surface film on the templates during the coating process, one side was masked with 3M cellulose tape prior to coating. Sodium hydroxide (NaOH) pellets were obtained from Mallinckrodt. Purified water was obtained by passing house-distilled water through a Milli-Q (Millipore) water purification system. Sandpaper (1500 grit, 3M) and quick-dry epoxy from Cole-Parmer Instrument Co. were used to prepare samples for electron microscopy studies. Formvar-coated 200 mesh copper grids were purchased from Ted Pella, Inc., and double-sided carbon disks were purchased from Electron Microscopy Sciences.

Synthetic Method. The perovskite nanotubes, fibers, and bulk powders were prepared from a 0.8 M chelate sol−gel. A 5% excess of lead was added to compensate for lead volatility, and the total volume of the solution was 10 mL. Because of the esterfication pathways of the chelate sol and its effect on microstructure, only fresh sols were used to fabricate tubes and fibers.[33,34] In a typical reaction, 4.779 g (12.59 mmol) of $Pb(CH_3CO_2)_2 \cdot 3H_2O$ were dissolved in 5 mL of acetic acid, refluxed at 60 °C for ∼20 min, and then allowed to cool to room temperature. A second solution of 4.083 g (11.99 mmol) of $Ti[O(CH_2)_3CH_3]_4$ and 2.5 mL of 1-butanol was prepared and added to the lead acetate solution leading to the formation of a clear sol. After the sol was prepared, the unmasked side of the template was coated by the dropwise addition of the sol. Through capillary action, the sol penetrated the nanochannels of the template. Excess sol was wiped off, and the template was allowed to dry in air for 30 min. Prior to the calcination process, templates were reinforced by inserting them between Al_2O_3 plates (dimensions of a microscope slide) and placed upright in a combustion boat. Samples were calcined in air at a rate of 50 °C/h to 650 °C and were kept at this temperature for 6 h before being slowly cooled to room temperature at a rate of 30 °C/h. The remaining unused sol was allowed to gel and was calcined using the same heating procedures as those to produce our "bulk" powders as the control samples. The bulk powder samples were calcined at the following temperatures: 450, 550, and 650 °C.

Characterization Methods. The morphologies and elemental compositions of the structures were investigated using a JEOL JSM6500F field-emission scanning electron microscope (SEM)

(9) Akdogan, E. K.; Safari, A. *12th IEEE Interanational Symposium on Applications of Ferroelectrics*, Honolulu, HI, 2001; pp 487−490.
(10) Baodong, Q.; Bin, J.; Yuguo, W.; Peilin, Z.; Weilie, Z. *Chin. Phys. Lett.* **1994**, *11*, 514−517.
(11) Chattopadhyay, S. *Nanostruct. Mater.* **1997**, *9*, 551−554.
(12) Chattopadhyay, S.; Ayyub, P.; Palkar, V. R.; Multani, M. *Phys. Rev. B* **1995**, *52*, 13177−13183.
(13) Fu, D.; Suzuki, H.; Ishikawa, K. *Phys. Rev. B* **2000**, *62*, 3125−3129.
(14) Ishikawa, K.; Yoshikawa, K.; Okada, N. *Phys. Rev. B* **1988**, *37*, 5852−5855.
(15) Jiang, B.; Peng, J. L.; Bursill, L. A.; Zhong, W. L. *J. Appl. Phys.* **2000**, *87*, 3462−3467.
(16) Ma, W.; Zhang, M.; Lu, Z. *Phys. Status Solidi A* **1988**, *166*, 811−815.
(17) Pandey, D.; Singh, N.; Mishra, S. K. *Indian J. Pure Appl. Phys.* **1994**, *32*, 616−623.
(18) Pramanik, P.; Das, R. N. *Mater. Sci. Eng., A* **2001**, *304−306*, 775−779.
(19) Wang, Y. G.; Zhong, W. L.; Zhang, P. L. *Soild State Commun.* **1994**, *90*, 329−332.
(20) Zhong, W. L.; Jiang, B.; Zhang, P. L.; Ma, J. M.; Cheng, H. M.; Yang, Z. H.; Li, L. X. *J. Phys.: Condens. Matter* **1993**, *5*, 2619−2624.
(21) Zhou, Q. F.; Zhang, J. X.; Chan, H. L. W.; Choy, C. L. *Ferroelectrics* **1997**, *195*, 221−214.
(22) Limmer, S. J.; Cao, G. *Adv. Mater.* **2003**, *15*, 427−431.
(23) Limmer, S. J.; Hubler, T. L.; Cao, G. *J. Sol.-Gel Sci. Technol.* **2003**, *26*, 577−581.
(24) Limmer, S. J.; Seraji, S.; Forbess, M. J.; Wu, Y.; Chou, T. P.; Nguyen, C.; Cao, G. *Adv. Mater.* **2001**, *13*, 1269−1272.
(25) Limmer, S. J.; Seraji, S.; Wu, Y.; Chou, T. P.; Nguyen, C.; Cao, G. *Adv. Funct. Mater.* **2002**, *12*, 59−64.
(26) Urban, J.; Yun, W. S.; Gu, Q.; Park, H. *J. Am. Chem. Soc.* **2002**, *124*, 1186−1187.
(27) Yun, W. S.; Urban, J. J.; Gu, Q.; Park, H. *Nano Lett.* **2002**, *2*, 447−450.
(28) Schaak, R. E.; Mallouk, T. *Chem. Mater.* **2000**, *12*, 3427−3434.
(29) Mao, Y.; Banerjee, S.; Wong, S. S. *Chem. Commun.* **2003**, 408−409.
(30) Akdogan, E. K.; Safri, A. *Jpn. J. Appl. Phys.* **2002**, *41*, 7170−7175.
(31) Li, S.; Condrate, R. A.; Spriggs, R. M. *Spectrosc. Lett.* **1988**, *21*, 969−973.
(32) Blum, J. B. *Mater. Lett.* **1985**, *3*, 360−362.
(33) Boyle, T. J.; Dimos, D.; Schwartz, R. W.; Alam, T. M.; Sinclair, M. B.; Buchheit, C. D. *J. Mater. Res.* **1997**, *12*, 1022−1030.
(34) Doeuff, S.; Dromzee, Y.; Taulelle, F.; Sanchez, C. *Inorg. Chem* **1989**, *28*, 4439−4445.

coupled with X-ray energy dispersive spectroscopy (EDS) from NORAN Vantage System. Pristine templates were coated with 5 nm of Au using an Anatech Hummer VII sputter coater prior to being attached to SEM stubs with double-sided carbon tape. Powders, tubes, and fibers were all examined without Au coating. Micrographs of the powders and fibers were obtained by spreading the calcined samples directly onto carbon tape. Images of the tubes were obtained by adhering the calcined AAO template containing our samples to a piece of paper towel embedded with epoxy. After the epoxy hardened, any perovskite surface film was removed by polishing. Then the AAO template was removed from the tubes by immersing the sample in 6 M NaOH for 6 h. The sample was rinsed several times with Millipore water until the filtrate pH reached 7. After drying overnight in air, the samples were attached to SEM stubs using double-sided carbon tape.

The microstructures of our materials were determined by transmission electron microscopy (TEM). Tubes were prepared for TEM in a manner similar to that described above without the application of an epoxy backing to the AAO template. After the dissolution in 6 M NaOH, the solution was decanted off after centrifugation and the remaining sample was rinsed several times with water. When the washings reached a neutral pH, the sample was sonicated to disperse the material in solution. A pipet was used to transfer an aliquot of sample water onto a Formvar-coated 200 mesh copper grid. The sample was allowed to dry overnight on the grid. The calcined nanofibers were also dispersed onto the TEM grids using the water/sonication technique. Images and selected-area electron diffraction (SAD) patterns were taken on a JEOL JEM 2000 EXII microscope. The accelerating voltage was 100 kV, and the camera length was 100 cm for the tubes and 80 cm for the fibers.

SAD patterns were evaluated by the method of comparative d spacings resulting in an error of 6%. Measurement of the radii was performed with a meteric ruler, and error associated with the measurement is ± 0.5 mm. The average crystal symmetry and dimension for the bulk and nanoscale material were found using powder X-ray diffraction (PXRD) patterns collected on a Scintag X2 diffractometer with Cu Kα radiation (1.5406 Å) and a Peltier detector. Samples were scanned at a rate of 0.02°/2 s in the 2θ range of 5−60°. The average crystallite size for the material was determined from the full width at half-maximum of the (111) reflection for the tetragonal phase and the (101) reflection for the cubic phase using the single line parametrized Warren−Averbach method.[35] Instrument broadening was corrected using NIST SRM 1976. Lattice parameters were calculated with the JADE software system.[36] Local crystal symmetry was evaluated by room-temperature Raman scattering on a home-built optical bench using an Acton Research Spectra Pro-275 LN_2-cooled charge-coupled device detector (256 × 1024) and controller model 51130 with an argon laser line at 514.5 nm. The system was calibrated with an argon pencil-style calibration lamp from ORIEL Instruments and a sulfur standard. Raman spectra were evaluated using the GRAMS/AI software system.[37] The ferroelectric−paraelectric (FE−PE) phase transition temperature (T_c) and enthalpy of phase transition (ΔH) were monitored by differential scanning calorimetery (DSC). Data were collected using a TA Instruments DSC 2929 Modulated differential scanning calorimeter under N_2 flow at 10 °C/min in the temperature range of 28−600 °C.

III. Results and Discussion

In reviewing the experimental literature on size effects upon the $PbTiO_3$ ferroelectric phase transition, it is difficult to determine an exact critical size. $PbTiO_3$ nanoparticles, with crystallites on the order of 8−200 nm, have been prepared by the sol−gel, chelate, nitrate, citrate, coprecipitation, Pechini, and injection−hydrolysis procedures, and various physical characterization and theoretical techniques have been employed to acquire the critical size.[8−17,19−21,31,32,38−42] Therefore, we compared our results of the nanotubes and fibers to those of control samples made with the same solution chemistry in the absence of any templates.

Morphologies and Microstructures of $PbTiO_3$ Bulk Powders, Nanotubes, and Nanofibers. Using electron microscopy, we determined that each template had an effect on the morphology and microstructure of the samples produced from the 0.8 M chelate sol. With powder processing and no template, the size and shape of the polycrystalline grains were controlled by the heating conditions as in the literature. SEM micrographs of the bulk powder, Figure 1, illustrate the effect of this methodology on grain growth after three heat treatments of 450, 550, and 650 °C. Grain sizes were measured from the images to be on average ∼0.1, 0.3, and 0.7 μm, respectively. The micrographs also illustrate that there was some distribution of grain sizes within each sample. To address this variable, our approach to investigating grain/crystallite size effects on the T_c and the critical size uses the systematic incorporation of membrane templates. In addition to the heating conditions, the templates serve as a second control over grain growth and distribution of grain size. Production of our 1-D perovskites was achieved by filling the channels of two types of porous membranes: anodized alumina films and track-etched PC films. If completely filled, each template has cylindrical nanochannels that will form fibers or tubes if incompletely filled.[1]

The nearly hexagonally closed packed pore surface of the pristine amorphous alumina (AAO) template is shown in Figure 2a. After the templates have been filled and heat-treated and their surface films removed by polishing, the nanostructures could be revealed when the AAO was removed with 6 M NaOH. SEM images, Figure 2b,c, show the top and side views of the calcined $PbTiO_3$ nanostructures that were yielded by our methods. Electron microscopy also revealed that the nanostructures prepared in AAO were typically tubes with outer diameters of ∼200 nm and lengths of ∼50 μm, corresponding to the dimensions of the template. The rounded or smooth filmlike features on top of the tube openings are a result of the incomplete removal of the $PbTiO_3$ surface film. Elemental analysis of the nanotubes determined by EDS showed emission lines associated with Pb, Ti, and O, and no emission lines from Al, confirming that the template had been removed. The TEM image and SAD pattern taken for a single $PbTiO_3$ nanotube, Figure 2d,

(35) Klug, H. P.; Alexander, L. E. *X-ray Diffraction Procedures For Polycrystalline and Amorphous Materials*, 2nd ed.; John Willey & Sons: New York, 1974.
(36) Jade software program, MDI, 1999, Livermore, CA.
(37) Grams/AI software suite, ThermoElectron Corp., 2001, San Jose, CA.
(38) O'Brien, S.; Brus, L.; Murray, C. B. *J. Am. Chem. Soc.* **2001**, *123*, 12085−12086.
(39) Schwartz, R. W. *Chem. Mater.* **1997**, *9*, 2325−2340.
(40) Shih, W. Y.; Shih, W.-H.; Akasay, I. A. *Phys. Rev. B: Condens. Matter* **1994**, *20*, 15575−15585.
(41) Yu, D. S.; Han, J. C.; Ba, L. *Am. Ceram. Soc. Bull.* **2002**, *81*, 38−39.
(42) Zhang, Q.; Whatmore, R.; Vickers, M. E. *J. Sol.-Gel Sci. Technol.* **1999**, *15*, 13−22.

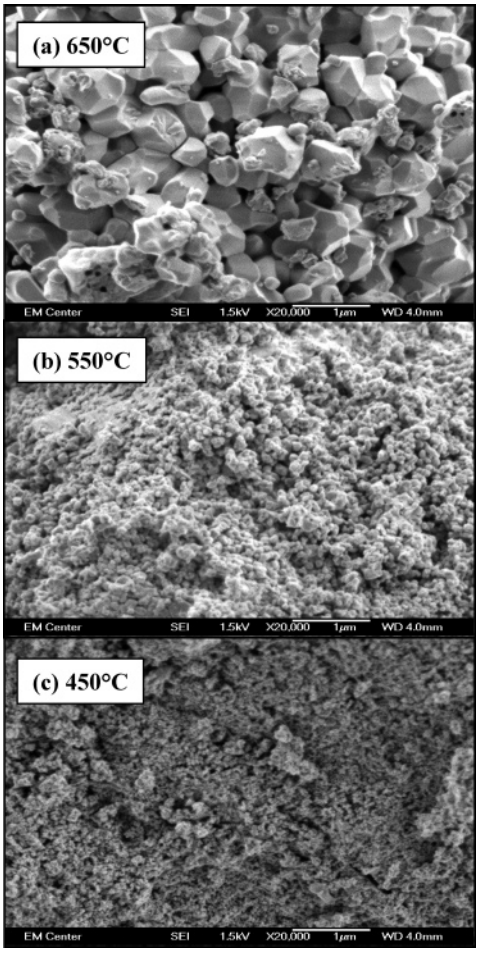

Figure 1. Field-emission SEM images of the $PbTiO_3$ bulk powder illustrating grain growth and morphologies obtained for calcination temperatures of (a) 650, (b) 550, and (c) 450 °C. Scale bar is 1 μm, and micrographs were taken at $\times$20 000.

revealed that the tubes comprised grains that were smaller than the 20-nm scale bar, and the electron diffraction ring patterns indicate that these tubes were polycrystalline.

Tube formation using the AAO template was the only nanostructure morphology resulting from our chelate sol−gel template method. Attempts to produce nanorods by allowing the template to soak in the sol for longer periods of time (e.g., 30 s to 5 min) or by changing the concentration of the sol from 0.3 to 0.8 M were unsuccessful and yielded only tubes. Previously, the formation of TiO_2 nanorods from tube structures was achieved when the template was in contact with a colloidal sol for increasing time periods; however, the sol used in our experiments was homogeneous, and stable colloidal sols did not readily form.[43] Analysis of SEM images revealed that varying the concentration of the Pb/Ti chelate sol did not have a significant effect on the tube wall thickness. One additional experiment, aimed at forming rods rather than tubes, was to build up the wall thickness by successive coatings of the template. As a result of the fragility of the AAO template, polishing of the surface films destroyed the template before it could be recoated.

The rough untreated surface of the track-etched PC membrane template, with its randomly distributed 200-nm pores, is shown in Figure 3a. This template was removed from the structures during the calcination process by combustion in air. Figure 3b is the SEM top view and Figure 3c is the side view of the resulting fiber structures formed within the 200-nm PC template when calcined at 650 °C. The prevention of surface film formation on one side of the membrane was achieved by masking. Figure 3c shows that the ~6-μm-long fibers were adhered to an ~1-μm thin film formed on the coated side. The grain sizes of the surface film were on average 0.75 μm. The TEM image and SAD pattern for a single $PbTiO_3$ nanofiber are shown in Figure 3d. Solid fibers comprised a string of individual grains that

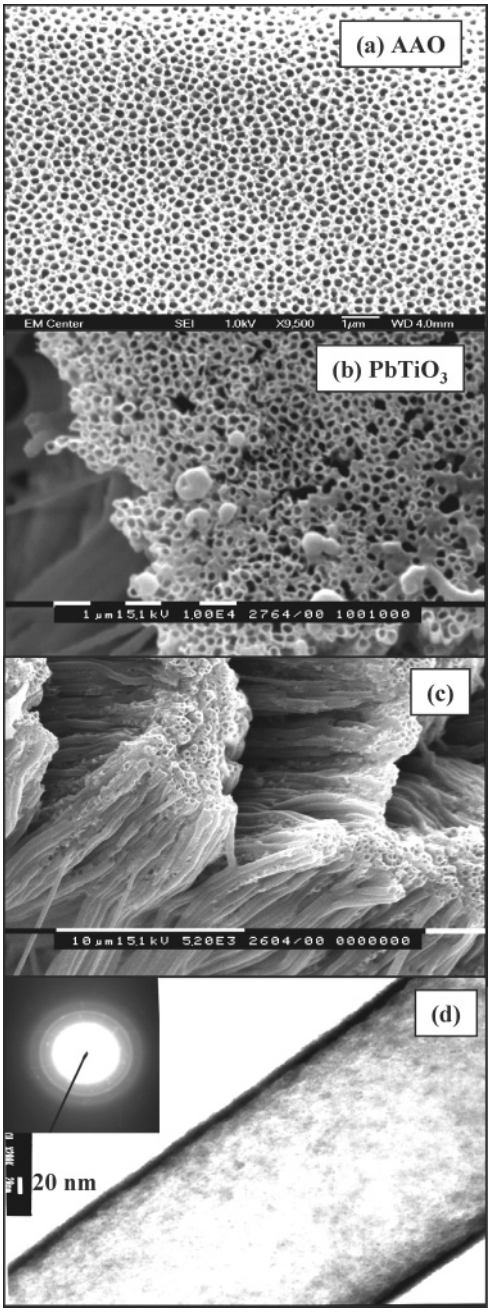

Figure 2. Field-emission SEM images of (a) the pristine surface of an AAO template and (b) the top view and (c) side view of calcined $PbTiO_3$ nanotubes, showing bundle formation after the removal of AAO. The tubes have an o.d. of 200 nm and are ~50-μm long. The TEM image (d) of a single nanotube shows that these structures comprise grains <20 nm, and the inset of the ring pattern indicates that the small grains are polycrystalline. Tubes shown were calcined at 650 °C.

(43) Lakshmi, B. B.; Patrissi, C. J.; Martin, C. R. *Chem. Mater.* **1997**, *9*, 2544−2550.

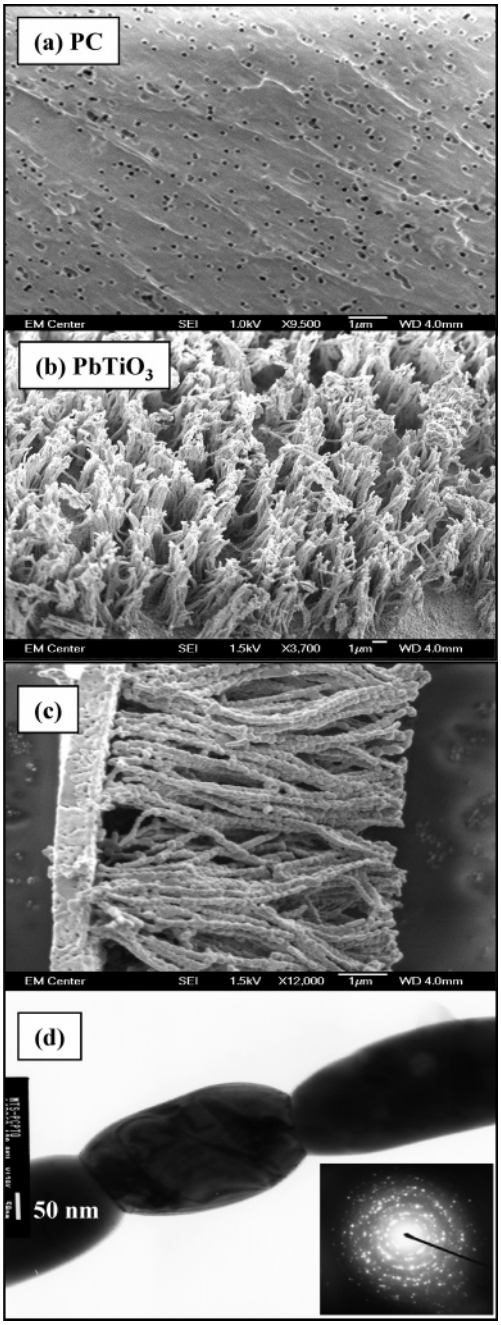

Figure 3. Field-emission SEM images of (a) the pristine surface of the 200-nm pore PC template, (b) the top view of $PbTiO_3$ nanofibers, and (c) the side view showing the attached (~6 μm) fibers to a 1-μm-thick surface film, after the removal of the template. The TEM image (d) confirms that the structures are solid and are made up of a string of grains ~200 nm in diameter. The inset shows that these grains are polycrystalline. Fibers shown were calcined at 650 °C.

were polycrystalline and varied in length but were ~200-nm wide in diameter.

The uniquely different morphologies and grain sizes of our nanostructures made from sols of the same concentrations but different templates illustrate a significant template effect. One explanation for fiber versus tube formation is the difference in the length of the nanochannels within the templates. Production of a fiber from tube morphology is a result of complete versus incomplete filling of the nanochannels within the template.[1−4] During our coating process, the sol entered the channels through capillary action. Each template used had hydrophilic surfaces, and uptake of a polar solution should have easily occurred. As the 0.8 M solution entered the 200-nm channels of different lengths (~50 μm for AAO and ~10 μm for PC), incomplete filling or coating of the AAO template for the longer channel may have resulted while complete filling was observed in the PC channel. In effect, the shorter channel length allowed for more solution to enter.

Table 1. Unit Cell Parameters and Crystallite Size Data for $PbTiO_3$[a,b]

material and processing temperature	*a* (Å)	*c* (Å)	*c*/*a*	*V* (Å^3)	crystallite size (nm)
ref 44	3.899	4.153	1.065	63.1	
650 °C powder	3.887(2)	4.132(5)	1.063	62.4	157
550 °C powder	3.894(1)	4.126(4)	1.060	62.6	49
450 °C powder	3.903(1)	4.132(4)	1.059	62.9	29
650 °C 50-nm fibers	3.906(1)	4.141(2)	1.060	63.2	53
650 °C 100-nm fibers	3.899(1)	4.128(1)	1.059	62.7	57
650 °C 200-nm fibers	3.899(1)	4.132(1)	1.060	62.8	73
ref 46	3.961		1.000	62.2	
650 °C 200-nm tubes	3.966(3)		1.000	62.4	11
650 °C thin film on AlOx	3.895(1)	4.113(1)	1.056	62.4	29

[a] Tetragonal crystallite size determined with the (111) reflection. [b] Cubic crystallite size determined with the (110) reflection.

In contrast to Limmer et al., our sintering profile of heating at 50 °C/h to 650 °C may also explain why our fibers have the "string" of grains morphology with diameters very close to the 200-nm template pore diameter. Recently, 200-nm PC templates were used in the growth of $BaTiO_3$, $Pb(Zr_{0.53}Ti_{0.48})O_3$, and other oxide nanorods using sol−gel electrophoresis.[22−25] The templated sols were heat-treated at 700 °C for 15 min. It was observed that the metal oxide rods produced from this flash heating method resulted in structures having rod diameters and grains significantly smaller than those of our fibers.[23,24] During the heating stage, the templated sol−gels underwent densification and shrinkage to produce rods ~125−180 nm in diameter. This flash heat treatment probably helped ensure the growth of smaller polycrystalline grains. We are currently investigating the effects of sol concentrations and flash heating on the formation of tubes with the PC templates.

Evaluating the Room-Temperature Lattice Structure of $PbTiO_3$ Powders, Tubes, and Fibers. The room-temperature crystalline symmetry of the nanotubes and fibers was determined by PXRD, electron diffraction, the method of comparative *d* spacings, and Raman spectroscopy. These methods were used to verify whether the templates used in this experiment were successful in both limiting grain/crystallite size and retaining the tetragonal ferroelectric phase.

PXRD. The average room-temperature crystal structure was evaluated with PXRD. Lattice parameters and average crystallite sizes calculated from the PXRD data are summarized in Table 1. Because the samples are polycrystalline, the grain sizes observed from the SEM data are not easily directly related to the PXRD analysis. PXRD is an average of crystalline particle sizes, whereas SEM reveals the sizes of all matter, crystalline or not. Bulk powders were calcined at 450, 550, and 650 °C, and their respective powder patterns, Figure 4, illustrate the effects of crystallite size on the relative intensity and broadening of the peaks. Each pattern was indexed to the tetragonal unit cell and space group *P*4/*mmm*

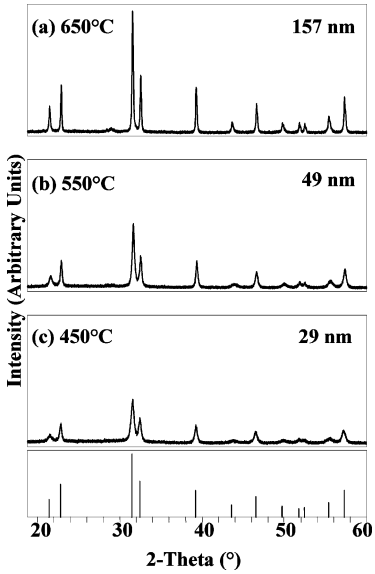

Figure 4. PXRD patterns for the bulk material calcined at (a) 650, (b) 550, and (c) 450 °C with 157-, 49-, and 29-nm crystallite sizes, respectively. Each sample was indexed to have the tetragonal phase and illustrates the effects of grain/crystallite size on the relative intensity and broadening of the peaks.

(123).[44] PbO (small broad peak $2\theta = 29°$) was observed in the bulk sample calcined at 650 °C.

The average crystallite sizes found within the grains of the bulk powders calculated from the (111) reflection using the single line parametrized Warren−Averbach method were 29 ± 3, 49 ± 5, and 157 ± 16 nm for the respective heating conditions. This method of analysis was used instead of the Scherrer method because it considers both microstrain and crystallite size, whereas the Scherrer equation assumes that loose powder is free of microstrain.[35,45] Akogdan's recent work on the measurement of critical size using diffraction techniques illustrated that the microstrain increased for $PbTiO_3$ nanoparticles < 75 nm and, therefore, is not negligible for mesocopic ferroelectrics when evaluating size.[8] In addition, the SEM images indicated that our powders were agglomerated and both tubes and fibers had grains that were under some strain to form the morphology; thus, we could not assume that microstrain had no effect. It was also determined that the average crystallite sizes calculated for the powders were smaller than the average grain size measured from the field-emission SEM image, Figure 1. This discrepancy implies that the grains of the bulk powders were composed of multiple crystals. The effect of crystallite size on the relative tetragonality (c/a) of each sample was monitored and compared to the $c/a = 1.065$ from the Powder Diffraction File file.[44] A decrease in the c/a of ~0.6, 0.5, and 0.2% was found for the powders with crystallite sizes of 29, 49, and 157 nm, respectively.

Diffraction patterns of the nanofibers, Figure 5, made from the 200-, 100-, and 50-nm pores of PC templates were also indexed to the tetragonal phase. Crystallite sizes for the fibers made from their respective templates were determined to be 72 ± 7, 57 ± 6, and 53 ± 5 nm, respectively. It is important

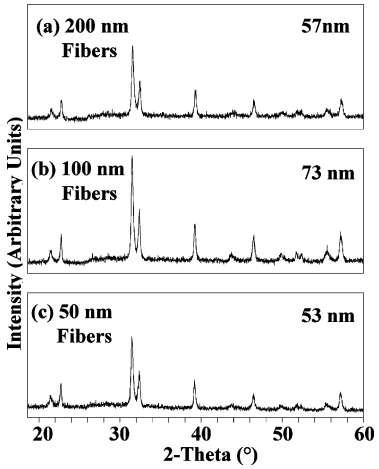

Figure 5. PXRD patterns of tetragonal $PbTiO_3$ fibers formed inside of (a) 0.2 μm (b) 0.1 μm and (c) 0.05 μm pore diameter PC templates calcined at 650 °C. Average crystallite sizes were determined to be 57, 73, and 53 nm for the respective sample size.

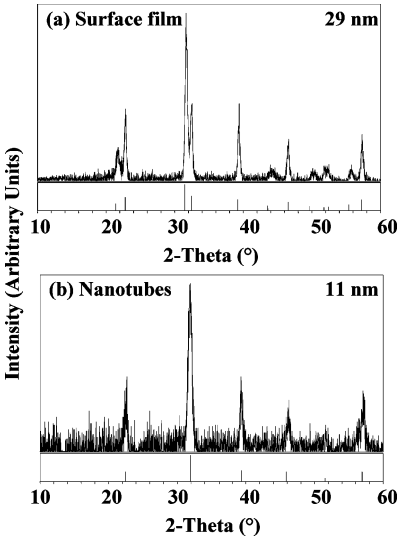

Figure 6. PXRD patterns for two phases obtained with samples made with AAO and calcined at 650 °C. Pattern a is of the residual surface thin film on the template after polishing and has the tetragonal phase. Pattern b is of the isolated nanotubes and has the cubic phase. Differences in the two phases are a result of the average crystallite size measured from the samples. The average crystallite size for the surface film was calculated to be 29 nm, whereas the tubes were 11 nm.

to note that these results are based on crystallites measured from fibers attached to a thin film, each with different grain sizes. The (c/a) values for the fibers were similar to the bulk powders having 29- and 49-nm crystallite sizes. Figure 6 shows that two displacive phases were obtained from the 200-nm AAO template. After calcination, the coated side of the AAO templates had a surface film with the tetragonal ferroelectric phase of $PbTiO_3$, an average crystallite size of 29 nm, and a $c/a = 1.056$. After the surface film was removed and the AAO dissolved, the sample was reevaluated. It was found to have the cubic paraelectric phase of $PbTiO_3$.[46] The (110) reflection was used to calculate an average crystallite size of 11 nm, in accordance with the grain size measurement from TEM, Figure 2d, and may be single-domain.[9] The conflicting analysis between the two PXRD

(44) JCPDS file 06-0452, International Centre for Diffraction Data, 1992.
(45) Cullity, B. D. *Elements of X-Ray Diffraction*; Addison-Wesley: Reading, MA, 1978.
(46) JCPDS file 40-0099, International Centre for Diffraction Data, 1992.

Table 2. Comparative *d*-Spacing Measurements for $PbTiO_3$ Nanotubes and Bulk Powder Calcined at 650 °C

ref 44 d spacing (XRD; Å)	measured *d* spacing (XRD; Å)	measured radius [SAD; mm (±0.5)]	calculated[a] *d* spacing (SAD; Å)
$d_{100} = 3.90$	$d_{100} = 3.87$	$r_{100} = 10.50$	$d_{100} = 3.90$
$d_{110} = 2.76$	$d_{110} = 2.75$	$r_{110} = 15.00$	$d_{110} = 2.73 \pm 0.17$
$d_{200} = 1.95$	$d_{200} = 1.94$	$r_{200} = 21.25$	$d_{200} = 1.93 \pm 0.12$
$d_{211} = 1.61$	$d_{211} = 1.60$	$r_{211} = 25.25$	$d_{211} = 1.62 \pm 0.10$

[a] First line assumed to be $d_{100} = 3.90$ from ref 44.

patterns are a result of the measured crystallite size for the nanotubes and surface film.

A limitation in using PXRD to evaluate nanoscale materials is the effect of line broadening that occurs as the particle or grain size decreases, thus, causing a pseudocubic structure to be oberved.[45] Therefore, a complementary evaluation was required to determine if the nanotubes were tetragonal. Table 2 lists the measured and calculated values for the tetragonal phase obtained from the PXRD data and the SAD ring pattern for the method of comparative *d* spacings. Comparing the observed ratios of the ring pattern radii, we concluded that they were close to the ratios of the literature and measured *d*-spacing values for the tetragonal phase. To confirm this result further, Raman scattering, which has shown to be more sensitive for the detection of tetragonal symmetry and phase transitions in nanoscale particles of $PbTiO_3$ and $BaTiO_3$, was used in conjunction with PXRD.[7]

Raman Spectroscopy. Table 3 summarizes the Raman spectroscopy results at room temperature confirming the crystal symmetry of the perovskites. The spectra for the bulk powders, Figure 7, have peaks that are assigned to the vibrational modes for tetragonal symmetry determined for single crystals of $PbTiO_3$.[47,48] Peaks marked with an asterisk are lattice modes that undergo changes resulting from both phase transformation and crystallite size. The $E + B_1$ is designated as a silent mode and appears to be independent of size effects and phase behavior. The effect of reducing crystallite size can be observed in two aspects of the spectra. The E(2TO) peak undergoes a decrease in its relative intensity, and the frequency of the low energy E(1TO) soft mode near 88 cm^{-1} decreases with line broadening. The E(1TO) mode is an indicator of phase transition and dielectric behavior.[49] These deviations were first reported in polycrystalline $PbTiO_3$ derived from sol−gel processing.[31,32]

Our bulk powders showed an E(1TO) mode frequency decrease from 88 to 86 cm^{-1} as the crystallite size was reduced. Spectra for the nanofibers and nanotubes produced from the 200-nm pore templates, Figure 8, confirm that they are tetragonal. Nanofibers made from 100- and 50-nm PC templates have spectral line shapes similar to that of the 200-nm sample. The fibers have E(1TO) frequencies of 88 cm^{-1} for crystallite sizes of 73 and 57 nm and 87 cm^{-1} for 53-nm crystallites. These results can be compared to Ishikawa et al.'s work wherein nanoparticles above 52 nm had no significant difference in Raman shift when compared to single-crystal data.[50] Observing lattice modes for tetragonal

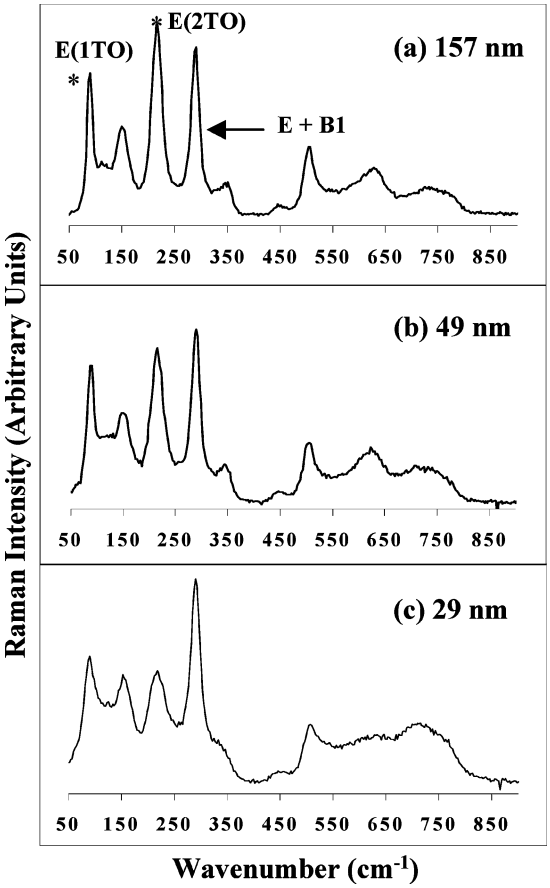

Figure 7. Room-temperature Raman spectra of the bulk powders with (a) 157-, (b) 49-, and (c) 29-nm crystallite sizes. The effects of reducing grain/crystallite size are seen with a decrease in relative intensity of the E(2TO) mode and frequency of the E(1TO) mode (marked with asterisks).

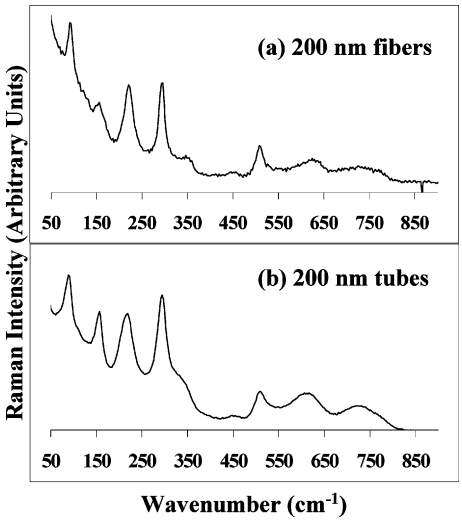

Figure 8. Room-temperature Raman spectra for the 200-nm $PbTiO_3$ (a) fibers and (b) tubes calcined at 650 °C verifying tetragonal symmetry in both samples.

symmetry for the nanotubes with an 11-nm crystallite size indicated that the tubes were in the ferroelectric phase and not in the paraelectric phase. The nanotubes had an E(1TO) frequency of 85 cm^{-1}. Similar room-temperature Raman spectra have been reported by Fu et al.[13] for nanocrystalline material made by sol−gel having a 17-nm average crystallite size and by Zhou et al. for 18-nm crystallites.[21] A broad and undefinable spectrum was also reported by Zhou et al. for a

(47) Burns, G.; Scott, B. A. *Phys. Rev. B* **1973**, *7*, 3088−3101.
(48) Frey, R. A.; Siberman, E. *Helv. Phys. Acta* **1976**, *49*, 1.
(49) Burns, G.; Scott, B. A. *Phys. Rev. Lett.* **1970**, *25*, 167−170.
(50) Ishikawa, K.; Yoshikawa, K.; Okada, N. *Phys. Rev. B* **1988**, *37*, 5852.

Table 3. Raman Scattering Data for $PbTiO_3$ Bulk Powders, Tubes, and Fibers

	PXRD									
sample material	symmetry	d_{XRD} (nm)	ν_1 (cm^{-1}) E1(TO)	ν_2 (cm^{-1}) A_1(1TO)	ν_3 (cm^{-1}) E(2TO)	ν_4 (cm^{-1}) E + B1	ν_5 (cm^{-1}) A_1(2TO)	ν_6 (cm^{-1})	ν_7 (cm^{-1}) E(3TO)	ν_8 (cm^{-1}) A_1(3TO)
650 °C powder	tetragonal	157	88	151	216	289	334	414	506	626
550 °C powder	tetragonal	49	88	151	216	289	344	447	507	615
450 °C powder	tetragonal	29	86	154	219	290			507	
650 °C	cubic	11	85	155	216	293		439	509	613
650 °C 200-nm fibers	tetragonal	73	88	152	219	290	347	449	508	612
650 °C 100-nm fibers	tetragonal	57	88	151	219	290	346	433	508	918
650 °C 50-nm fibers	tetragonal	53	87	151	218	290			507	623

sample with 15-nm crystallite size.[21] In comparing the effects of crystallite size on the E(1TO) mode for the tubes and the fibers, we found that the soft mode frequency is less than the reported single-crystal frequency of 89 cm^{-1} but not significantly different from our control samples. The nanotubes, which displayed the lowest frequency, were comparable to Zhou's data for an 18-nm crystallite size of E(1TO) = 84 cm^{-1}, whereas the 15-nm crystallite size had an E(1TO) mode of 74 cm^{-1} determined from the peak fitting of a poorly resolved spectrum.[21]

In contrast to single-crystal data under ambient conditions, these Raman shifts are the most distinct feature for nanoparticulate polycrystalline powders. Burns and Scott demonstrated, using in situ temperature experiments, that there was a temperature dependence on mode strength for $PbTiO_3$ single crystals. They observed that as the Curie temperature (T_c = 493 °C) was approached, the E(1TO) soft mode, located at 89 cm^{-1}, moved toward lower energy.[47] This frequency change also occurred with high-pressure experiments which forced the tetragonal system toward the cubic phase.[51] The decrease in E(1TO) frequency with nanocrystalline material under ambient conditions has been attributed to an increase in surface tension as nanoparticles become smaller. It has been postulated that a decrease in frequency coupled to particle size could be due to hydrostatic pressure created by surface tension.[16,21,32] The studies compared their nanocrystalline $PbTiO_3$ powders to single crystals that were placed under hydrostatic pressure. Blum's data were compared to a single crystal that was under 1 GPa.[51] Ma reported that particles with ~40-nm crystallites had Raman scattering frequencies similar to those of a single crystal under 2 GPa with an E(1TO) = 78 cm^{-1}. Hydrostatic pressure has also been used to explain phonon mode behaviors observed with thin films of $PbTiO_3$ deposited on Pt/Si substrates.[52] Fu et al. reported that $PbTiO_3$ films with an average grain size of 47 nm had E(1TO) = 80 cm^{-1} (~1.35 GPa). The studies concluded that because nanocrystals have a large surface-to-volume ratio, the large surface tension could cause internal stress analogous to the hydrostatic pressure effect on single crystals. Our results confirm a slight decrease in energy but do not show that the crystallites in our nanostructures are undergoing internal stresses equivalent to 1−2 GPa.

The results of both the X-ray diffraction and the Raman scattering experiments demonstrated that the templates and chemistry used were successful in obtaining the ferroelectric phase in confined 1-D materials. Analysis of the effects of crystallite size on the tetragonal crystal system of our samples indicates that deviations from unit cell parameters occurred. The largest tetragonal lattice strain, ~0.6%, was observed in our bulk powders and fibers, and the cubic lattice was determined for our nanotubes. Our data indicate that the stresses of surface-to-volume ratio of our grains on the crystallites are not equal to the 2 GPa reported by Ma and Zhou. On the basis of the electron micrograph results that both fibers and tubes are geometries composed of grains, which should be under a certain amount of "hydrostatic pressure", we would expect to see larger deviations in the E(1TO) soft mode frequency, especially for the nanotubes.

There are two explanations for the deviation from Ma and Zhou's hypotheses. First, the soft mode frequency shifts may result from the larger grain/crystallite sizes of the minor surface film that remain on our tube samples and thin film attached to the fibers; therefore, the E(1TO) frequency of the nanotubes and fibers appeared similar to the bulk powders. Second, under ambient conditions, the decrease in soft mode frequency due to hydrostatic pressure on the individual grains created by surface tension is not as dramatic as previously reported and may be misleading. Recently, Akdogan and Safri confirmed the latter explanation. They reported that the $(c/a) \rightarrow 1$ with decreasing particle size could not be attributed to surface effects because the requirement of several billion pascals of pressure created by the surface itself was a physically unrealistic situation.[30]

In research on nanoparticles, it is generally accepted that the spherical particle model is appropriate because it is unbound and relieved of the microstrains that occur with thin films because of grain boundaries and internal stresses; however, a drawback to this approach is that agglomeration of the particles does occur as seen with our bulk powders, Figure 1. Thus nanoparticles are not entirely free of these constraints. To understand the cause of ferroelectric reduction, the core of the nanoparticle and not its surface tension needs to be evaluated.[30]

Phase Transformation Behavior of $PbTiO_3$ Powders, Tubes, and Fibers. The effects of aspect ratio and crystallite size upon the ferroelectric phase transition were monitored through DSC which provides an indirect measurement of the polarization.[53] Aspect ratio, which is defined at the length/diameter of the structure, was varied by the template used. Aspect ratios evaluated were 250 for AAO and 200, 100, and 50 for the PC templates.

(51) Sanjurjo, J. A.; Lopez-Cruz, E.; Burns, G. *Phys. Rev. B* **1983**, *28*, 7260−7268.
(52) Fu, D. S.; Iwadaki, H.; Ishikawa, K. *J. Phys.: Condens. Matter* **2000**, *12*, 399−414.
(53) Asiaie, R.; Zhu, W.; Akbar, S. A.; Dutta, P. K. *Chem. Mater.* **1996**, *8*, 226−234.

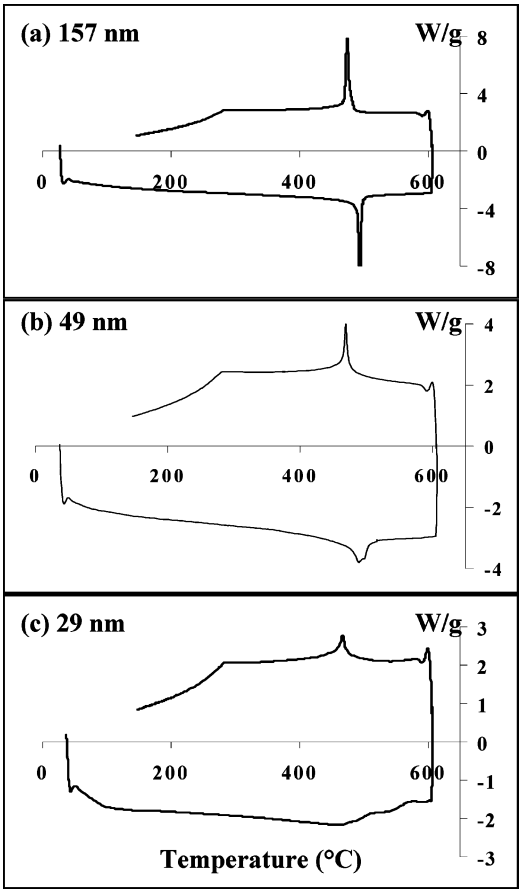

Figure 9. DSC scans of bulk $PbTiO_3$ powder with (a) 157-, (b) 49-, and (c) 29-nm crystallite sizes. The effect of reducing grain and crystallite size upon the Curie transition temperature (T_c), enthalpy of phase transition (ΔH), and hysteresis of phase behavior is shown.

DSC. As a second control, bulk powders that were treated at identical temperatures and conditions as the membrane-bound nanotubes were also treated with 6 M NaOH, filtered, and washed. DSC data showed no difference in T_c or ΔH. Thermal hysteresis and the effects of crystallite size on the ferroelectric phase transition are shown in Figure 9 for bulk $PbTiO_3$ powders. Ferroelectric perovskites undergo displacive transitions that are reversible. Our traces show the tetragonal (ferroelectric) phase being heated, the endotherms resulting from the phase transition to cubic symmetry, and the exotherm for the cubic PE−FE transition that occurs when cooled through the Curie temperature.

Table 4 summarizes the FE−PE Curie temperature (T_{c1}) that occurs upon heating, its reverse (T_{c2}), and their respective ΔH values. These data confirm decreases in both T_c and ΔH for the bulk samples. As the crystallite size decreases, the endo- and exotherms become broader and the limitation of DSC is shown. When the 29-nm crystallite size does not have a distinct FE−PE T_c upon heating, however, the effects of annealing are seen with a discernible PE−FE transition upon cooling. Figure 10 displays the representative traces for the 200-nm fibers and the 200-nm tubes made by our template method. DSC thermograms for the 100- and 50-nm $PbTiO_3$ fibers calcined at 650 °C had T_c and ΔH similar to the bulk powders with a 49-nm crystallite size. Our results indicate that crystallite size and not aspect ratio of our 1-D fibers contributed to a change in ferroelectricity. Examination

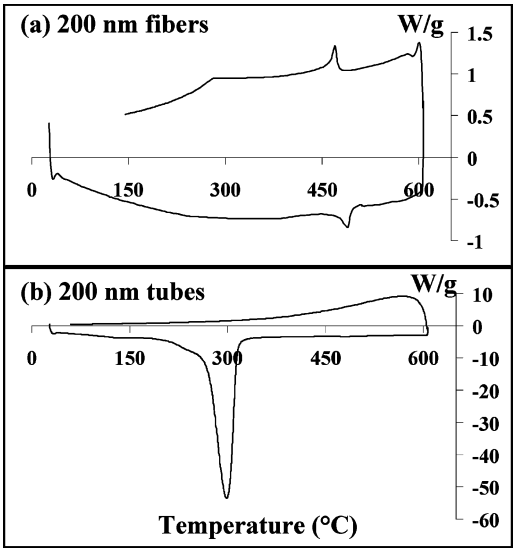

Figure 10. DSC traces of the 200-nm $PbTiO_3$ (a) fibers and (b) tubes calcined at 650 °C. Thermal hysteresis of phase change is only observed in the fibers.

of the nanotubes showed that the crystallite size was too small to evaluate with DSC.

We previously reported that $PbTiO_3$ nanotubes had a T_c of 234 °C for a sample having a crystallite size of 11 nm and that nanotubes of $PbZrO_3$ and PZT had similar deviations from the bulk phase transition temperature.[54] Upon further examination, only endotherms ranging from about 123−266 °C were observed upon heating with no reverse exotherms as seen in Figure 10b for the materials made with the AAO template. Therefore, we could not assign this endotherm as a ferroelectric phase transition. A second cyclic DSC scan on the same sample of $PbTiO_3$ nanotubes used in Figure 10b was performed to see if the heat treatment had an annealing effect on the crystals that would allow for a transition to be monitored by DSC. The results showed no indication of thermal hysteresis associated with displacive phase transformation as seen with our bulk powder and nanofibers.

Performing the first and second cyclic DSC scans within the temperature range of 493 °C for the nanotubes and observing no annealing effects may invalidate our first assumption: the surface film caused the tetragonal lattice modes to be observed during our Raman experiment. PXRD analysis confirmed that the surface film had an average crystallite size of 30 nm. Our DSC trace of the bulk powders with an average crystallite size of 29 nm indicated that annealing effects took place and displayed an exotherm attributable to the PE−FE transition. If our nanotube sample contained a large fraction of the 30-nm crystallites from the surface film, these crystals would have been detected during the DSC analysis.

Thermogravametric Analysis (TGA) and Mass Spectrometry. TGA results are shown in Figure 11a for the $PbTiO_3$ nanotubes calcined at 650 °C, removed from the AAO template with NaOH, rinsed, and dried in an oven at 100 °C overnight. A weight loss of ∼20% had taken place around

(54) Chang, K.-S.; Hernandez, B. A.; Fisher, E. R.; Dorhout, P. K. *J. Korean Chem. Soc.* **2002**, *46*, 242−251.

Table 4. Differential Scanning Calorimeter Data for $PbTiO_3$ Bulk Powder and Fibers

material and processing temperature	crystallite size d_{XRD} (nm)	aspect ratio	T_{c1} (°C) FE−PE	T_{c2} (°C) PE−FE	ΔH_1 (J/g)	ΔH_2 (J/g)
650 °C powder	157		494	474	5.1	5.1
550 °C powder	49		490	469	2.8	2.0
450 °C powder	29			468		0.86
650 °C 200-nm fibers	73	50	489	470	2.7	1.8
650 °C 100-nm fibers	57	100	490	469	1.6	1.4
650 °C 50-nm fibers	53	200	490	468	2.4	1.5

234 °C. The mass spectrum, Figure 11b, contained peaks for H_2O ($m/z = 18$) and OH ($m/z = 17$). It was determined that our process for removing the AAO template and the capillary action of the nanotubes allowed water to be stored within them even upon drying. This resulted in the observation of endotherms to occur between 120 and 266 °C. The temperature ranges for water evaporation from the tubes were associated with the amount of time they had contact with water. The TGA results indicate that nanotube structures may offer unique storage capabilities for water and other materials.

Understanding how the phase transition temperature (T_c) and enthalpy of transition (ΔH) are influenced by particle size could explain how the spontaneous polarization is affected. According to eq 1,

$$\Delta H = 2\pi P^2 T_c / C \quad (1)$$

ΔH is related to the polarization (P), the Curie−Weiss constant (C), and the transition temperature (T_c). From eq 1, it can be seen that a decrease of P and T_c will lead to a decrease in ΔH. One explanation for the effects of depolarization has been discussed in terms of a randomly oriented surface charge layer that begins to take precedence over the highly ordered ferroelectric interior as the size of a particle becomes smaller.[53] Eventually, the particle reaches a critical size where polarization becomes zero because of the removal of the ferroelectric core. Using Landau−Devonshire theory,

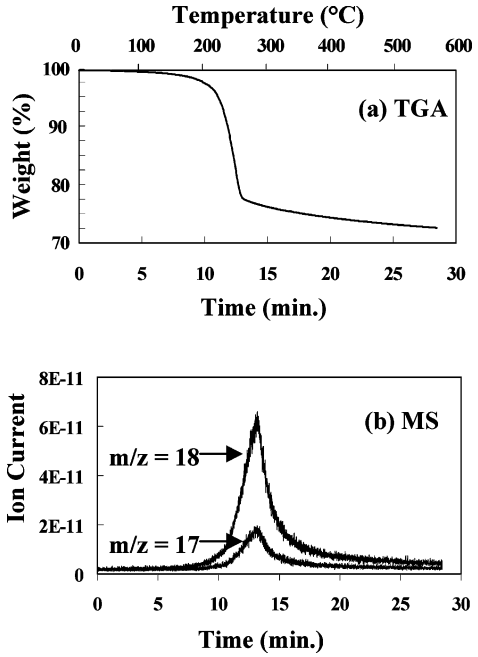

Figure 11. (a) TGA of the tubes calcined at 650 °C shows that a weight loss of 20% occurred during the temperature range for the endotherm. (b) Mass spectrometry of the weight loss shows water ($m/z = 18$) as the source of the endotherm.

Wang et al. were able to explain this phenomenon and predicted a critical size of 4.2 nm for $PbTiO_3$ particles.[19] This size is smaller than Ishikawa et al.'s experimental value of 13.8 nm observed while monitoring T_c by Raman scattering and Akdogan and Safri's extrapolated value of 15 nm by PXRD.[9,14] It should be noted, however, that, in all the reported transition temperatures for sol−gel derived $PbTiO_3$ nanocrystals using DSC, no T_c was reported below 400 °C.[10−12]

In determining the effects of hydrostatic pressures and temperature on dielectric constants, Samara showed that a single crystal of $PbTiO_3$ had a $T_c = 323$ °C when placed under ~2.4 GPa.[55] Fu and co-workers have reported a T_c below 400 °C with nanoparticles; however, this was demonstrated through an in situ Raman temperature experiment wherein crystals with an average size of 7 nm began to show peaks associated with tetragonal symmetry at a T_c of 166 °C.[13] At this temperature, the authors suggested that the 7-nm nanocrystals underwent a phase transition from orthorhombic to tetragonal which implies that a stable orthorhombic phase existed before reaching tetragonal symmetry. The orthorhombic−tetragonal phase transition is never seen in the $PbTiO_3$ system; however, evidence of such behavior has been seen in the $BaTiO_3$ system. Frey and Payne's work on submicrometer $BaTiO_3$ particles showed evidence of Raman active modes arising from orthorhombic symmetry before reaching the tetragonal phase as a function of grain size.[7] Our experiment with the nanotubes showed that measurement of crystallite sizes of perovskites smaller than 20 nm may require scanning probe techniques or in situ Raman temperature experiments to correctly evaluate the polarization of the material and phase transition.

IV. Summary

We have used the sol−gel template synthesis method to fabricate 1-D perovskite materials and have shown that they are useful models for the investigation of size effects on aspect ratio and dimensionality on ferroelectricity. Ferroelectric $PbTiO_3$ nanotubes and fibers, made within AAO and PC membranes, were used to study the effects of crystallite size on both lattice structure and polarization. Comparisons between a control group of bulk powders, tubes, and fibers were made. We found that tetragonality (c/a) and phase transition temperatures (T_c) of our polycrystalline models for fibers and powders deviated from the single-crystal data but were similar to each other on the basis of crystallite size. The crystallite size of the nanotubes may have hindered the ability to indirectly measure polarization with DSC. Results

(55) Samara, G. A. *AIP Conf. Proc.* **2000**, *535*, 344−353.

from DSC measurements appear to indicate that crystallite size plays a larger role than aspect ratio on ferroelectricity. We also serendipitously found that nanotube structures are useful in the storage of liquids such as H_2O. Finally, our analysis of the E(1TO) soft mode frequency also showed that the crystallites in our structures were not under the hydrostatic pressures of 1−2 GPa that have previously been reported. In examining the phase transitions associated with the changes of particle size, our Raman studies demonstrated that surface tension considerations may be less important than the local structure of the Ti^{4+}. Thus, the ferroelectric particle core and crystal symmetry are likely more relevant in determining a mechanism for size effects with pervoskite materials.

Acknowledgment. We wish to thank John Chandler of the Electron Microscopy Center along with Ana Kanevce of the Physics Department at Colorado State University for their technical support. We also acknowledge funding from the Department of Energy ER45791. B.A.H.-S. acknowledges The Colorado AGEP for support.

CM0493896